Personalized Fusion of Ultrasound and Electromyography-derived Neuromuscular Features Increases Prediction Accuracy of Ankle Moment during Plantarflexion

Qiang Zhang[1], William H. Clark[2], Jason R. Franz[2], Nitin Sharma[1*]

[1]Joint Department of Biomedical Engineering, University of North Carolina at Chapel Hill and North Carolina State University, 4212 Engineering Building III, Raleigh, NC 27606, USA; and

[2]Joint Department of Biomedical Engineering, University of North Carolina at Chapel Hill and North Carolina State University, 152 MacNider Hall, Chapel Hill, NC 27599, USA

*Author for correspondence

Nitin Sharma

Email: nsharm23@ncsu.edu

1840 Entrepreneur Dr.

4212C Engineering Building III

Raleigh, NC 27695

Abstract

Objective: Compared to mechanical signals that are used for estimating human limb motion intention, non-invasive surface electromyography (sEMG) is a preferred signal in human-robotic systems. However, noise interference, crosstalk from adjacent muscle groups, and an inability to measure deeper muscle tissues are disadvantageous to sEMG's reliable use. In this work, we hypothesize that a fusion between sEMG and *in vivo* ultrasound (US) imaging will result in more accurate detection of ankle movement intention.

Methods: Nine young able-bodied participants were included to volitionally perform isometric plantarflexion tasks with different fixed-end ankle postures, while the sEMG and US imaging data of plantarflexors were synchronously collected. We created three dominant feature sets, sole sEMG feature set, sole US feature set, and sEMG-US feature fusion set, to calibrate and validate a support vector machine regression model (SVR) and a feedforward neural network model (FFNN) with labeled net moment measurements.

Results: The results showed that, compared to the sole sEMG feature set, the sEMG-US fusion set reduced the average net moment prediction error by 35.7% ($p<0.05$), when using SVR, and by 21.5% ($p<0.05$), when using FFNN. In SVR, the sole US feature set reduced the prediction error by 24.9% ($p<0.05$) when compared to the sole sEMG feature set. In FFNN, the sEMG-US fusion set reduced the prediction error by 28.2% ($p<0.05$) when compared to the sole US feature set.

Conclusion: These findings indicate that the combination of sEMG signals and US imaging is a superior sensing modality for predicting human plantarflexion intention and can enable future clinical rehabilitation devices.

***Keywords*--- Ultrasound imaging, surface electromyography, isometric ankle plantarflexion, support vector machine regression, feedforward neural network, human effort prediction**

Abbreviations and Acronyms

sEMG	Surface electromyography
US	Ultrasound
LG	Lateral gastrocnemius
MG	Medial gastrocnemius
SOL	Soleus
PA	Pennation angle
FL	Fascicle length
SVM	Support vector machine
SVR	Support vector machine regression
FFNN	Feedforward neural network
IRB	Institutional Review Board
MVIC	Maximum volitional isometric contraction
RMSE	Root mean square error
PCC^2	Squared Pearson correlation coefficient
MAV	Mean absolute value
ZC	Zero crossing
SSC	Slope sign change
WL	Waveform length
MRMS	Moving root mean square
ROI	Region of interest
ANOVA	Analysis of variance
Tukey's HSD	post-hoc Tukey's honestly significant difference tests
η_p^2	Effect sizes
d	Cohen's d
GAS	Gastrocnemius
HNM	Hill-type neuromuscular model

1 Introduction

The human ankle plantar flexor muscles generate a large burst of mechanical power during “push-off” to propel the body’s center of mass during locomotor tasks. Weakness or dysfunction of the plantar flexor muscles, for example, due to neurological disorders or injuries, causes dramatic reductions in this “push-off” power, thereby impairing normal walking and increased metabolic energy costs [1]. Recent neurorehabilitation techniques to improve the diminished ankle plantar flexors function mainly focus on using powered ankle exoskeletons [2]–[4] and functional electrical stimulation [5], [6]. To maximize patient benefits from neurorehabilitation, the wearers need to be actively involved in the training and effectively engaged with the robotic devices. Thereafter, intuitive human-in-the-loop control strategies are required to generate efficient and effective assistance for the wearers to optimize specific task performance. One representative control strategy, known as assist-as-needed control [7], [8], depends on accurately determining volitional human motion intention. Conventional means to approximate limb motion intention include mechanical sensors (e.g., force, torque) installed on a rigid frame. These exoskeletal sensors are subject to inaccuracies due to an inevitable misalignment between the exoskeletal and biological joint centers, thus inducing undesired interaction forces [9], [10].

In recent decades, non-invasive neuromuscular signals have been investigated to estimate human limb motion intention. As a widely used neuromuscular signal, surface electromyography (sEMG) measures electrical potentials arising from activated alpha motor neurons. The amplitude and frequency of sEMG signals are positively related to the intended muscle activation level [11]. For example, neuromuscular model-based methods or model-free calibrations to associate sEMG signals with joint mechanical function (e.g., joint moment [11]–[13] or angular position [14]) can estimate limb movement intention. This neuromuscular signals-based limb movement intention detection approach could minimize the interaction between the wearable sensor and human joint, avoid the misalignment issue mentioned above, and provide the physiological response when investigating volitional limb movement. However, there are several shortcomings for sEMG-based human intention detection, such as interference from adjacent muscles when capturing EMG signals and an inability to measure deeply-located

muscles [15], [16]. Alternatively, two-dimensional B-mode ultrasound (US) imaging is another non-invasive methodology that overcomes the aforementioned sEMG shortcomings of electrical noise and interference due to the direct visualization of the targeted skeletal muscles measured from US imaging. US imaging's structural and functional features have been studied to understand measured muscle activities and predict human volitional muscle contraction force or joint moment. The most frequently used structural features from US images include pennation angle (PA) [13], [17], fascicle length (FL) [18], muscle thickness [19], and cross-sectional area [20]. Apart from these structural features from US imaging, functional features, including static and dynamic image pixel analysis (known as echogenicity and speckle tracking), have also been investigated to correlate with muscle or joint mechanical functions [11], [21]–[23].

Most of the aforementioned sEMG and/or US imaging-related contributions focused on a single superficial skeletal muscle, and few studies have investigated the application to synergistic superficial and deep skeletal muscles to estimate human joint volitional effort. Besides, although neuromuscular signals from sEMG and US imaging have been fused to predict ankle joint volitional dorsiflexion moments [11], [13], few studies have investigated ankle joint plantarflexion volitional effort by using sEMG and US imaging fusion. The potential benefits of combining different neuromuscular signals from plantar flexor muscles, like the improvement of human motor intention prediction accuracy, the mitigation of the sEMG-induced interference, and the reduction of US imaging-derived feature drift during cyclic muscle contraction, remain unexplored. In the current work, our primary goal was to investigate the performance of human volitional net plantarflexion moment prediction by using a fusion between personalized sEMG dominant features and personalized US imaging dominant features. We used support vector machine (SVM) analysis, a popular non-parametric machine learning tool for both classification and regression [24], to build the mapping between neuromuscular feature sets and net plantarflexion moment. The support vector machine regression (SVR) model with a linear kernel function was employed due to its simplicity, computational efficiency, and unique optimal solution. We hypothesized that using the calibrated SVR model, the sEMG-US imaging feature fusion would reduce the prediction error of the volitional net plantarflexion moment, compared to the dominant feature sets from sole sEMG or sole US imaging. We collected synchronized

sEMG signals and US images from individual plantar flexor muscles that operate at different depths (e.g., LG, MG, and SOL). We determined the dominant features from the sEMG signal and US images from the correlation analysis between each feature and measured net plantarflexion moment. Specifically, three feature sets were established for the SVR model calibration and net plantarflexion moment prediction, including an sEMG-US imaging feature fusion set, a sole sEMG feature set, and a sole US imaging feature set. Furthermore, the prediction results by using an SVR model were compared with those by using a feedforward neural network (FFNN) model.

2 Materials and Methods

2.1 Subjects and experimental protocol

The study was approved by the Institutional Review Board (IRB) at the University of North Carolina at Chapel Hill (16-0379). An a priori power analysis of the repeated-measure analysis of variance (ANOVA) determined that at n = 9 subjects would have 86.8 % power to detect ($p<0.05$) a difference in the isometric ankle joint moment prediction by using different neuromuscular feature sets (i.e., with an moderate effect size of 0.3). This study uses data from nine participants, five males and four females (Age: 25.3$\pm$5.8 years, Height: 1.74$\pm$0.08 m, Mass: 66.8$\pm$8.2 kg), without any neuromuscular or orthopedic disorders within the last six months. Every participant was familiarized with the experimental procedures and signed an informed consent form before participating in the experiments.

The experimental setup for this study is illustrated in Fig. 1 (a). Each participant sat comfortably on a dynamometer (Biodex, Shirly, NY, USA), with the right foot secured to the dynamometer pedal. A supporting frame stabilized the right thigh to eliminate the contributions from proximal muscle groups while performing plantarflexion. The knee flexed to replicate that near the push-off phase of walking (~20°). The participants performed three ramped volitional isometric plantarflexion at each of five ankle joint postures (from 10° dorsiflexion to 30° plantarflexion in 10° increments). The order of those five ankle joint postures was randomly chosen for each participant. To elicit a symmetric loading-unloading profile, participants started from rest and increased their net plantarflexion moment until the maximum effort to determine the maximum volitional isometric contraction (MVIC) within the first 2-second duration. After

the MVIC, participants returned to rest within the second 2-second duration. Participants performed the ramp loading procedure following verbal encouragement to reach MVIC. Before data collection, participants briefly practiced the isometric plantarflexion tasks using a real-time display of their net ankle moment. The MVIC moment was defined as the peak across the three repetitions. We provided the participants with at least one minute for rest between two successive contraction trials to avoid muscle fatigue.

During all trials, a 60 mm linear array US transducer (Echoblaster 128, 7 MHz, Telemed, Vilnius, Lithuania) placed over the mid-belly of the right MG recorded B-mode US images at 61 frames per second through an image depth of 65 mm. This Telemed transducer placement and depth also enabled the imaging of the soleus muscle in the same image plane. We attached two differential sEMG sensors (Trigno TM Avanti Platform, DELSYS, MA, USA) to the LG and SOL muscles to non-invasively measure sEMG signals during plantarflexion. Since the relatively large US probe was attached to the MG, the remaining free space was very limited for the sEMG sensor setup, so we recorded LG sEMG signals. We recorded the ankle joint net plantarflexion moment from the Biodex dynamometer.

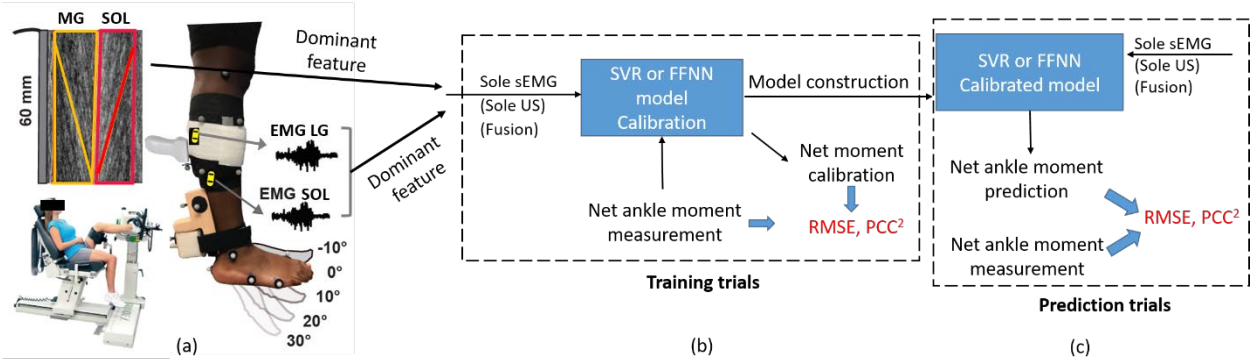

Figure 1: Summary of experimental protocol, measurements, and support vector machine regression (SVR) model calibration and net plantarflexion moment prediction. (a) Schematic of the experimental setup at five different ankle postures where participants performed isometric plantarflexion tasks. A single ultrasound (US) transducer was used to image both medial gastrocnemius (MG) and soleus (SOL) muscles with the appropriate probe placement. Two surface electromyography (sEMG) sensors recorded the electrical signals from LG and soleus (SOL) muscles. (b) Diagram of machine learning models (SVR and FFNN) calibration and evaluation with the calculation of root mean squared error (RMSE) and squared Pearson correlation coefficient (PCC^2). (c) Diagram of net plantarflexion moment prediction and evaluation based on machine learning models.

2.2 Data Acquisition and Processing

We synchronized signals from the Biodex and sEMG sensors at 1000 Hz using a real-time system programmed in LabVIEW (NI PCI 7352, National Instruments, TX, USA). Signals from the sEMG sensors were processed by an input module and the main amplifier (Trigno TM Avanti Platform, DELSYS, MA, USA) and filtered to the bandwidth between 20 Hz and 450 Hz. Signals from the dynamometer torque sensor were filtered using 4th order low-pass Butterworth filter with a cutoff frequency of 100 Hz. Besides, we synchronized binary ultrasound signals (i.e., signals indicating the start and stop of the collection) from the transducer at 1000 Hz using a waveform generator (SDG1025, SIGLENT, Shenzhen, China).

Five classic time-domain features were extracted from the filtered sEMG signals from both GS and SOL muscles, including mean absolute value (MAV), zero crossings (ZC), slope sign changes (SSC), waveform length (WL) [16], and moving root mean square (MRMS) [13], and their calculations are given by:

$$\begin{aligned} MAV(t_k) &= \frac{1}{L}\sum_{i=t_k-L+1}^{t_k}|x_i| \\ ZC(t_k) &= \sum_{i=t_k-L+2}^{t_k} sgn(-x_i x_{i-1}) \\ SSC(t_k) &= \sum_{i=t_k-L+2}^{t_k} sgn[(x_i - x_{i-1})(x_i - x_{i+1})] \\ WL(t_k) &= \sum_{i=t_k-L+2}^{t_k}|x_i - x_{i-1}| \\ MRMS(t_k) &= \sqrt{\frac{1}{L}\sum_{i=t_k-L+1}^{t_k} {x_i}^2} \end{aligned} \tag{1}$$

where *L* is the moving window length and x_i is the filtered sEMG signal at each sampling instant. The window length *L* is one essential parameter that affects the shapes of sEMG time-domain features thus affects the correlation between sEMG time-domain features and net plantarflexion moment. For each experimental trial, *L* was determined by maximizing the squared Pearson

correlation coefficients (PCC^2) between the sEMG time-domain features and the net plantarflexion moment. Since the sampling frequency of the sEMG signal is 1000 Hz, we selected *L* increasing from 2 ms to 1000 ms, and the corresponding PCC^2 values between each sEMG feature and plantarflexion moment were compared for each trial at each ankle joint posture on each participant. To balance the variation of *L* across different sEMG features, different ankle postures, different trials, and different participants, a consistent approximation of *L* for all participants was selected as 400 ms.

Following previously outlined techniques [25], the same investigator tracked all muscle PA and FL temporal data using an open-source MATLAB routine that employs an affine extension to an optical flow algorithm [26]. As shown in Fig. 2, we defined the fascicle length for one representative fascicle in the mid-belly of MG (FL_{MG}) and SOL (FL_{SOL}) from the superficial to the deep aponeurosis of each muscle. We defined PA of MG and SOL (PA_{MG} and PA_{SOL}) as the angle between each muscle fascicle and its corresponding deep aponeurosis. Additionally, we determined the echogenicity of the selected MG and SOL muscles by taking the mean echo intensity of corresponded ROIs (between 0 to 255, black = 0, white = 255), noted as $Echo_{MG}$ and $Echo_{SOL}$. Echogenicity, as a functional feature of US imaging using static pixel information without dynamic tracking performance, represents an averaged visualization change of the ROIs during the isometric plantarflexion process.

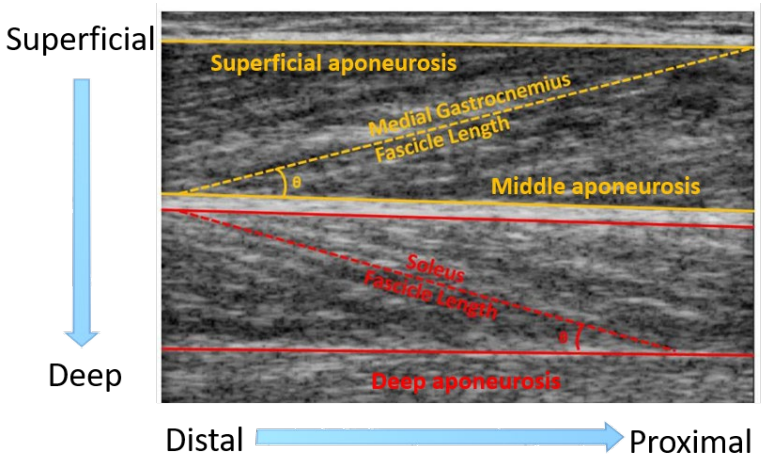

Figure 2: A typical US imaging B-mode frame for the MG and SOL muscles. Please note that this image is cropped to better view muscle features.

To summarize the data processing section, for both the gastrocnemius (GAS) and SOL muscles, temporal sEMG features and US imaging features were derived as $MAV(t_k)$, $ZC(t_k)$, $SSC(t_k)$, $WL(t_k)$, $MRMS(t_k)$, $FL(t_k)$, $PA(t_k)$, and $Echo(t_k)$. A correlation analysis between each temporal neuromuscular feature and the temporal net plantarflexion moment was used to determine two dominant features from both sEMG and US imaging signals, then to reduce the input dimensions and increase the calculation speed of the SVR model. Before that, the temporal US imaging features were linearly interpolated to 1000 Hz, thus guaranteeing the synchronization between each temporal neuromuscular feature and the temporal net plantarflexion moment. Finally, three feature sets were determined, e.g., sEMG dominant feature set, US imaging dominant feature set, and sEMG-US imaging feature fusion set.

2.3 Model calibration, prediction, evaluation, and statistical analysis

Although the Hill-type neuromuscular model has been well applied for the biomechanics community, it requires many physiological assumptions, complex system optimization, and model parameters identification when encountering muscle synergy or co-contraction problems. To avoid the physiology-based modeling procedures, both SVR and FFNN models were applied in this work. The SVR is, in essence, a non-parametric machine learning method especially aiming at samples with limited sizes. Based on the structural risk minimization, the SVR model is believed to obtain a globally optimal solution, instead of a local extremum and poor explanation ability behind the black box-like in an FFNN model. As shown in Fig. 3, the structure of the applied SVR model is similar to a multi-layer FFNN model with three hidden layers, where the number and function of each hidden layer are equal to those of the support vectors. The input layers from the left to right represent the sEMG dominant feature sets from GAS and SOL muscles, x_1^a and x_2^a, the US imaging dominant feature sets from GAS and SOL muscles, x_1^b and x_2^b, and the sEMG-US imaging feature fusion set, x_1^a, x_2^a, x_1^b, and x_2^b. It should be noted that the entire model structure of each SVR is adaptively generated directly, which means the number of support vectors is determined automatically by the adaptive SVR algorithm.

Naturally, the complexity of the SVR algorithm is independent of each input layer dimension and it is only related to the number of “support vectors” and also the kernel function

$\varphi(\cdot)$, which is selected as a linear kernel in this work for simplification. As described in Fig. 3, the input layers of SVR models realize the nonlinear mapping with the help of kernel function, and the linear mapping of the output $T(\cdot)$ is achieved also based on the kernel function. The searching procedure of an optimal solution is equivalent to solving the quadratic programming problem, which was solved by *quadprog* function in MATLAB. Parameters of $W_{(\cdot)}$ and $B_{(\cdot)}$ are the weight and polarization bias matrices from the feature space to output $T(\cdot)$, respectively, as described in Fig. 3.

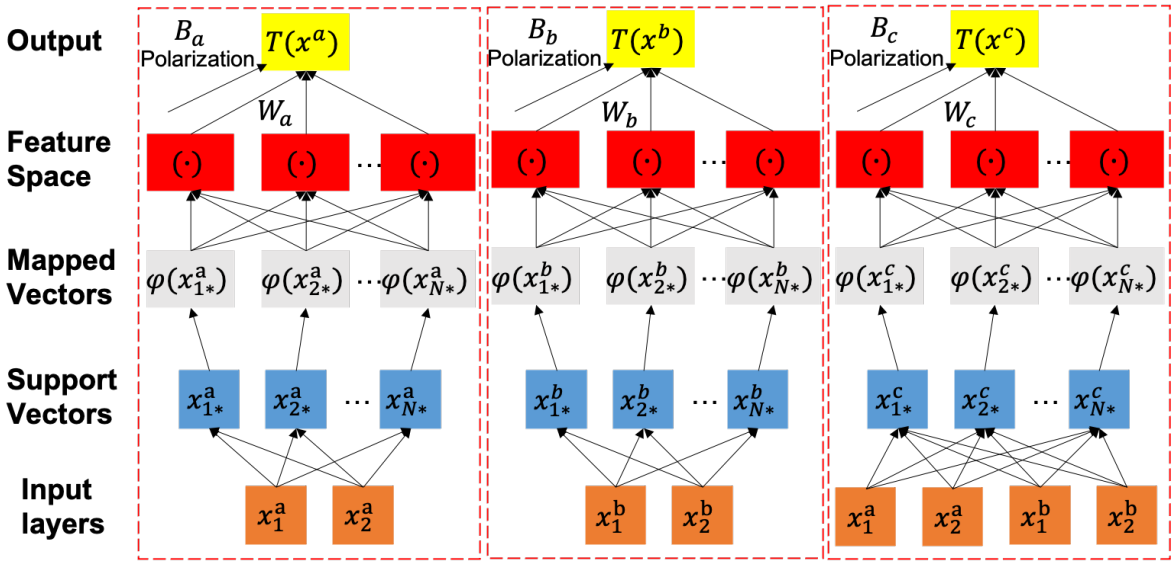

Figure 3. Support vector machine regression structure with three dominant feature sets from GAS and SOL.

Correspondingly, the deep FFNN was designed with three hidden layers and one output layer with neuron numbers of 5, 10, 5, and 1. The calibration was based on the Levenberg-Marquardt algorithm to get the optimized weight matrices and bias between every two layers. More detailed parameters and calibration procedure settings of the SVR and FFNN models can be found in the supplementary file. For each ankle joint posture, the SVR and FFNN models were calibrated by the three feature sets separately with data from randomly selected two plantarflexion trials. Data of the three feature sets from the remaining trial was used for net moment prediction based on the calibrated models. Three performance criteria were used to evaluate the SVR or FFNN model-based calibration and prediction of the net plantarflexion moment, including root mean square error (RMSE), normalized root mean square error (NRMSE), and PCC^2, as given below:

$$RMSE = \sqrt{\frac{1}{N}\sum_{i=1}^{N}(T_i - \hat{T}_i)^2} \quad (2)$$

$$NRMSE = \frac{\sqrt{\frac{1}{N}\sum_{i=1}^{N}(T_i - \hat{T}_i)^2}}{MVIC} \times 100 \quad (3)$$

$$PCC^2 = \frac{\left(\sum_{i=1}^{N}(T_i - \bar{T})(\hat{T}_i - \bar{\hat{T}})\right)^2}{\sum_{i=1}^{N}(T_i - \bar{T})^2 \sum_{i=1}^{N}(\hat{T}_i - \bar{\hat{T}})^2} \quad (4)$$

where T_i denotes each measured net plantarflexion moment, and $\hat{T}_i$ denotes each estimated moment with different feature sets in the calibration/prediction procedure, respectively. $\bar{T}$ denotes the average measured net moment, and $\bar{\hat{T}}$ denotes the average estimated net moment with different feature sets in the calibration/prediction procedure, respectively. Due to the MVIC deviation among individual participants, the NRMSE value can be used to compare the calibration and prediction results showing different ranges of fluctuation across individuals. The PCC^2 measures the extent of a linear relationship between the measured and estimated net moment in both calibration and prediction procedures.

Shapiro-Wilk parametric hypothesis test was used to determine the normality of the 45 NRMSE (PCC^2) values (1 trial × 5 ankle postures × 9 participants) in both calibration and prediction by applying those three feature sets, respectively. We performed statistical tests on the three groups of NRMSE (PCC^2) values in calibration and prediction. According to the Shapiro-Wilk test results, a one-way repeated-measure analysis of variance (ANOVA) or a Kruskal-Wallis test was used to determine if there was a significant difference among those three group's NRMSE (PCC^2) values either in calibration or prediction. When the significant main effects were identified, post-hoc Tukey's honestly significant difference tests (Tukey's HSD) were applied to determine the significant difference between every two NRMSE (PCC^2) groups out of three. The significant difference level was chosen as $p<0.05$ for all statistical tests. Effect sizes are reported as η_p^2 and Cohen's d for main effects from ANOVA or Kruskal-Wallis test and pairwise comparisons from Tukey's HSD, respectively.

3 Results

3.1 Plantarflexion moment at MVIC as a function of ankle posture

We observed significant ankle posture-dependent variations in net plantarflexion MVIC moment for all participants, as shown in Fig. 4. The results indicate for each individual, the net plantarflexion MVIC moment is largest at 10° of dorsiflexion and smallest at 30° of plantarflexion. Compared to the neutral ankle posture, plantarflexion MVIC moment averaged between 7.7% and 48.8% larger at 10° dorsiflexion and averaged between 5.1% and 26.5%, 7.5% and 40.1%, and 12.5% and 62.8% smaller at 10°, 20°, and 30° plantarflexion, respectively.

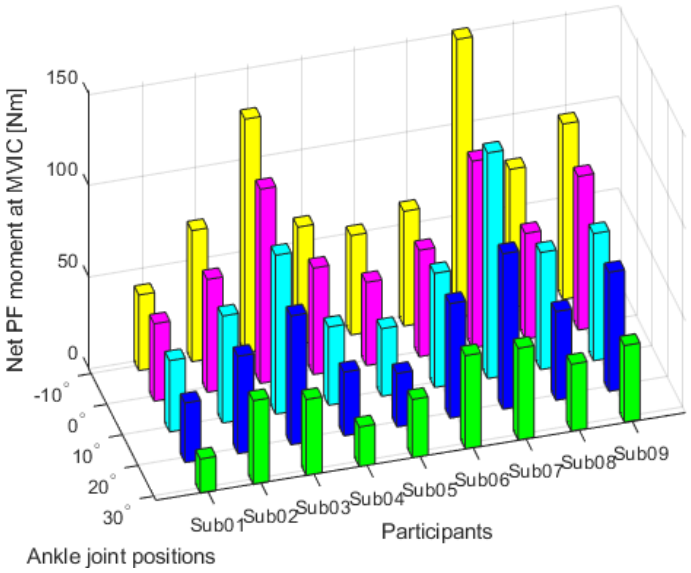

3.2 Dominant neuromuscular features determination

The results from correlation analysis are shown in Table 1, where the PCC^2 between each US imaging feature and net plantarflexion moment was calculated 15 times (3 trials × 5 ankle postures) for each participant. The reported values represent the average and standard deviation among those 15 PCC^2 values. The dominant features with the two highest averaged PCC^2 values are labeled as the bold numbers in Table 1. Apart from FL_{MG} on Sub02 and PA_{SOL} on Sub08, all other dominant US imaging features on each participant exhibit strong correlations with the net plantarflexion moment, with averaged PCC^2 values higher than 0.8.

Table 1: Squared Pearson correlation coefficient (PCC^2) values (average ± standard deviation) between each US imaging-derived feature and net plantarflexion moment across postures and trials on each participant.

Bold numbers represent the two selected dominant US features for each participant with the two highest PCC^2 values.

Participant	Squared Pearson correlation coefficients (PCC^2) with net plantarflexion moment					
	PCC^2 - FL_{MG}	PCC^2 - FL_{SOL}	PCC^2 - PA_{MG}	PCC^2 - PA_{SOL}	PCC^2 - $Echo_{MG}$	PCC^2 - $Echo_{SOL}$
Sub01	0.890 (0.076)	**0.956** (0.025)	0.460 (0.250)	**0.958** (0.026)	0.531 (0.249)	0.841 (0.050)
Sub02	**0.799** (0.134)	**0.891** (0.089)	0.405 (0.346)	0.755 (0.119)	0.392 (0.281)	0.733 (0.186)
Sub03	0.903 (0.073)	**0.961** (0.021)	0.431 (0.335)	**0.949** (0.044)	0.476 (0.352)	0.872 (0.129)
Sub04	**0.880** (0.084)	**0.921** (0.090)	0.749 (0.150)	0.870 (0.128)	0.246 (0.295)	0.359 (0.308)
Sub05	0.585 (0.242)	**0.869** (0.127)	0.715 (0.152)	**0.919** (0.047)	0.469 (0.247)	0.711 (0.216)
Sub06	0.854 (0.084)	**0.892** (0.057)	0.527 (0.262)	0.889 (0.078)	0.766 (0.135)	**0.932** (0.054)
Sub07	**0.825** (0.197)	0.635 (0.348)	0.587 (0.179)	0.659 (0.210)	0.724 (0.171)	**0.866** (0.118)
Sub08	0.586 (0.251)	**0.863** (0.155)	0.649 (0.294)	**0.775** (0.202)	0.389 (0.309)	0.578 (0.324)
Sub09	0.491 (0.355)	0.718 (0.261)	0.231 (0.222)	**0.805** (0.228)	0.467 (0.274)	**0.917** (0.083)

For sEMG signals, using the moving window length as 400 ms, the correlation analysis between each time-domain feature and net plantarflexion moment was conducted 15 times (3 trials × 5 ankle postures) for each participant. By comparing the averaged value from the 15 PCC^2 values related to each sEMG time-domain feature, the two dominant features were determined as the ZC_{LG} and ZC_{SOL}. The average and standard deviation of those 15 PCC^2 values between dominant sEMG features and net plantarflexion moment are listed in Table 2. We observed that apart from Sub02 and Sub03, all averaged PCC^2 values between ZC_{LG} or ZC_{SOL} and net plantarflexion moment were higher than 0.8. Besides, the difference between the averaged PCC^2 - ZC_{LG} and the averaged PCC^2 - ZC_{SOL} for each participant was modest, which indicates a consistent dominant sEMG time-domain feature among different participants. The results from Table 1 and Table 2 reveal strong linear correlations between the dominant neuromuscular features and net plantarflexion moment.

Table 2: PCC^2 values (Average ± Standard deviation) between each sEMG dominant feature and net plantarflexion moment across postures and trials on each participant. Bold numbers represent the two selected dominant sEMG time-domain features for each participant with the two highest PCC^2 values.

Participant	Sub01	Sub02	Sub03	Sub04	Sub05	Sub06	Sub07	Sub08	Sub09
PCC^2 - ZC_{LG}	**0.885** (0.040)	**0.693** (0.132)	**0.775** (0.111)	**0.825** (0.072)	**0.867** (0.079)	**0.887** (0.041)	**0.901** (0.037)	**0.914** (0.044)	**0.931** (0.020)
PCC^2 - ZC_{SOL}	**0.885** (0.040)	**0.693** (0.131)	**0.774** (0.112)	**0.826** (0.072)	**0.869** (0.078)	**0.887** (0.041)	**0.900** (0.037)	**0.914** (0.043)	**0.931** (0.019)

From the above results, three feature sets, including the sEMG set (two dominant features), US imaging set (two dominant features), and sEMG-US imaging fusion set (four dominant features), were determined. The sEMG dominant time-domain features, US imaging dominant features, and net plantarflexion moment measurement from one representative trial for Sub05 are shown in Fig. 5. The curves in Fig. 5 represent a positive correlation between net plantarflexion moment and ZC_{LG}, ZC_{SOL}, and PA_{MG}, respectively, and a negative correlation between net plantarflexion moment and FL_{SOL}. Results from other participants also show a positive correlation between net plantarflexion moment and PA_{SOL}, and a negative correlation between net plantarflexion moment and FL_{MG}, $Echo_{MG}$, or $Echo_{SOL}$, respectively.

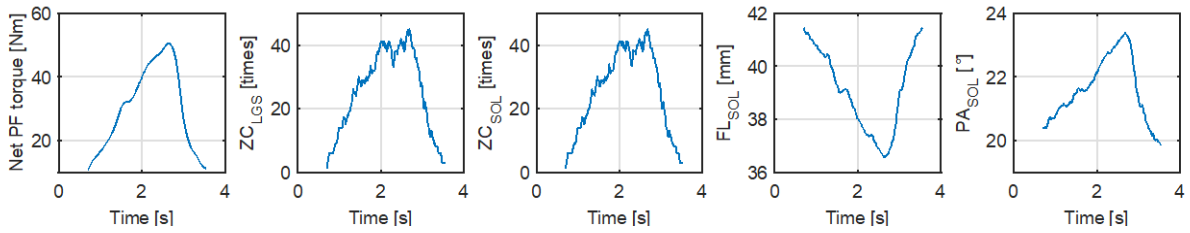

Figure 5: The temporal net plantarflexion moment measurements, dominant sEMG time-domain features, and dominant US imaging features at 10° dorsiflexion posture in trial 1 on Sub05.

3.3 Results of the ankle joint net moment prediction

From the above results, we could potentially anticipate that more accurate net plantarflexion moment prediction could be achieved by fusing dominant features from both sEMG signals and US imaging. When evaluating the SVR or FFNN model-based net moment prediction, for convenient notation, the RMSE between sEMG feature set-based calibration (or

prediction) and measured moment, between US imaging feature set-based calibration (or prediction) and measured moment, and between sEMG-US imaging fusion-based calibration (or prediction) and measured moment were denoted by $RMSE_{sEMG}$, $RMSE_{US}$, and $RMSE_{Fusion}$, respectively. Similarly, we also denote PCC^2_{sEMG}, PCC^2_{US}, and PCC^2_{Fusion} for their respective calibration and prediction procedures.

All calibration results are attached to the supplementary file, and the following results show prediction performance by using both SVR and FFNN models. Due to the space limitation, Fig. 6 only shows the SVR model-based net moment prediction and measured net moment in the remaining trial out of those three at the neutral ankle joint posture for all nine participants (results at other joint postures are in the supplementary file). In each subplot, the lateral axis represents the cycle percentage of the loading and unloading on the dynamometer in the prediction trial, while the axial axis represents the net plantarflexion moment. Prediction results from other ankle joint postures are similar to those summarized in Fig. 6. In prediction, $RMSE_{sEMG}$, $RMSE_{US}$, and $RMSE_{Fusion}$ at the five ankle joint postures across all nine participants are summarized in Fig. 7. After calculating the PCC^2 values and the normalized RMSE values at each posture to the corresponded net plantarflexion MVIC moment as shown in Fig. 4 (known as NRMSE), the Shapiro-Wilk test results showed that the NRMSE values and PCC^2 values across ankle postures and participants were normally distributed by using three neuromuscular feature sets. The results of ANOVA indicated the NRMSE values in prediction were significantly affected by feature sets (main effect, $p<0.05$, $\eta_p^2=0.22$), as well as the PCC^2 values (main effect, $p<0.05$, $\eta_p^2=0.38$). The statistical results of the prediction NRMSE values across the different ankle joint postures and participants are presented in Fig. 8 (a). By using the sEMG-US feature fusion set and US feature set, the net plantarflexion moment prediction NRMSE values were significantly reduced by 35.7% ($p<0.05$, d=-1.48) and 24.9% ($p<0.05$, d=-0.91), respectively, compared to that by using sole sEMG feature set. However, we did not observe a statistically significant difference between NRMSE values by using the sEMG-US fusion set and sole US feature set, although the mean NRMSE value was reduced ($p=0.182$, d=-0.49). Statistical results in Fig. 8 (b) show that by using the sEMG-US feature fusion set and the US feature set, the PCC^2 values between the moment prediction and moment measurement are 15.5% ($p<0.05$, d=0.88) and 14.9% ($p<0.05$,

d=0.76) larger than that using sole sEMG feature set, respectively. However, we did not observe a statistically significant difference between PCC^2 values by using the sEMG-US feature fusion set and sole US feature set, although the mean PCC^2 value was improved (p=0.932, d=0.05).

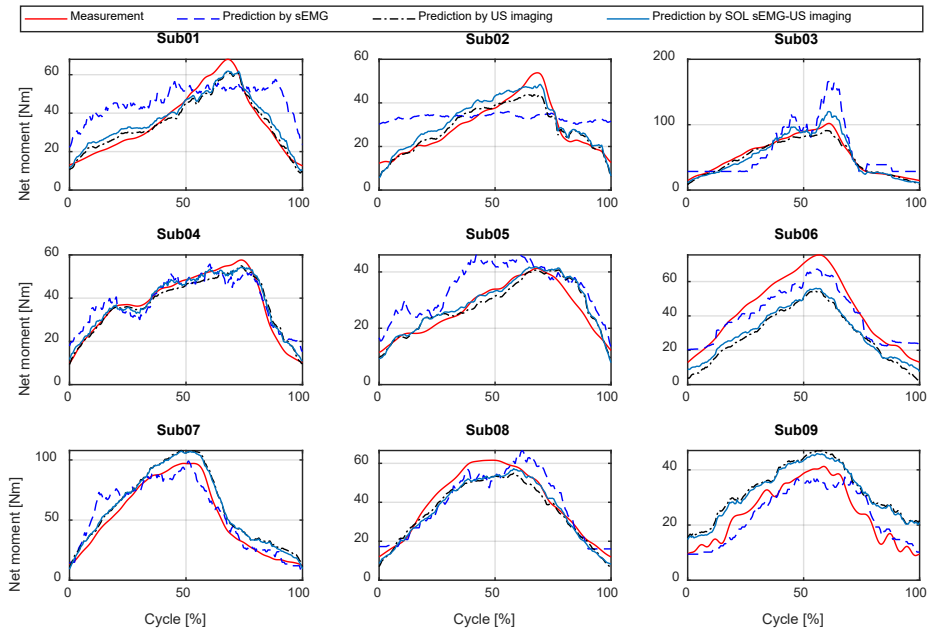

Figure 6: Net plantarflexion moment measurements and one trial prediction from the SVR model by using three dominant neuromuscular feature sets at the ankle joint neutral posture for all nine participants.

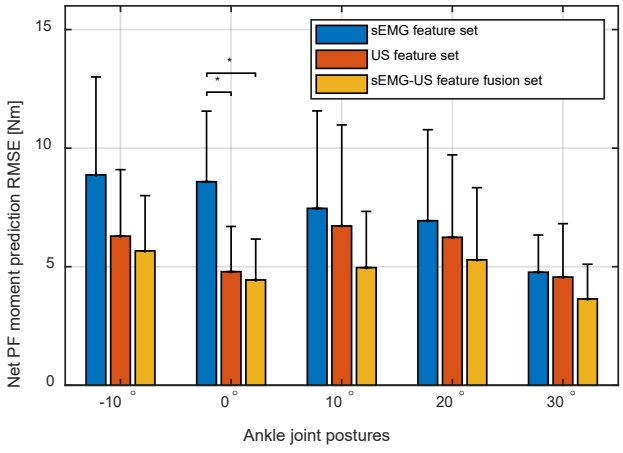

Figure 7: Net plantarflexion moment RMSE values in SVR prediction by using the three neuromuscular feature sets at five ankle joint postures across all nine participants.

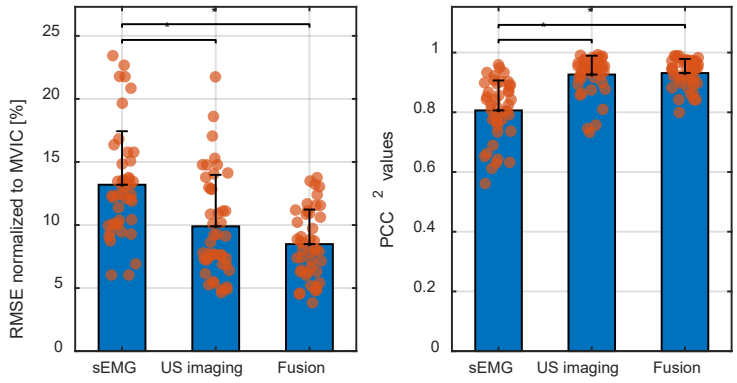

(a) (b)

Figure 8: Average and standard deviation of NRMSE values between the SVR prediction and net plantarflexion moment measurement in the left figure (a). Average and standard deviation of PCC^2 values between the prediction and net plantarflexion moment measurement in the right figure (b). Scattered data are collected from prediction procedures at all ankle joint postures across all participants. Asterisks (*) represents significant difference is at $p<0.05$.

Similarly, when the FFNN model was applied, the Shapiro-Wilk test results showed that the NRMSE values and PCC^2 values of each of the neuromuscular feature sets were normally distributed across ankle postures and participants. The results of ANOVA indicated that the NRMSE values in prediction were significantly affected by feature sets (main effect, $p<0.05$, η_p^2=0.20), as well as the PCC^2 values (main effect, $p<0.05$, η_p^2=0.36). The statistical results of the prediction NRMSE values across the different ankle joint postures and participants are presented in Fig. 9 (a). By using the sEMG-US feature fusion set, the net plantarflexion moment prediction NRMSE values were significantly reduced by 21.5% ($p<0.05$, d=-1.02) and 28.2% ($p<0.05$, d=-1.22), respectively, compared to that by using the sole sEMG feature set and sole US feature set. However, we did not observe a statistically significant difference between NRMSE values by using the sole sEMG feature set and sole US imaging feature set ($p=0.388$, d=0.35). Statistical results in Fig. 9 (b) show that by using the sEMG-US feature fusion set, the PCC^2 values between the predicted and measured moments are 13.1% ($p<0.05$, d=0.91) and 12.4% ($p<0.05$, d=0.86) larger than that using the sole sEMG feature set and US feature set, respectively. However, we did not observe a statistically significant difference between PCC^2 values by using the sole sEMG fusion set and sole US imaging feature set ($p=0.953$, d=0.07).

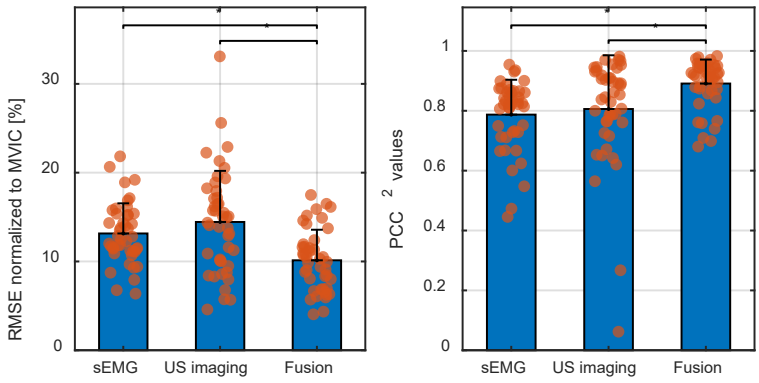

(a) (b)

Figure 9: Average and standard deviation of NRMSE values between the FFNN prediction and net plantarflexion moment measurement in the left figure (a). Average and standard deviation of PCC^2 values between the prediction and net plantarflexion moment measurement in the right figure (b). Scattered data are collected from prediction procedures at all ankle joint postures across all participants.

By comparing the calibration and prediction performance of the SVR and FFNN models, we observed that in calibration, FFNN significantly reduced the NRMSE values compared to SVR, when using the sEMG feature set ($p<0.05$), US imaging feature set ($p<0.05$), and sEMG-US imaging fusion set ($p<0.05$). Also, FFNN significantly increased the PCC^2 values compared to SVR, when using the sEMG feature set ($p<0.05$), US imaging feature set ($p<0.05$), and sEMG-US imaging fusion set ($p<0.05$). However, we observed that in prediction, SVR significantly reduced the NRMSE values compared to FFNN, when using the US imaging feature set ($p<0.05$), and the sEMG-US imaging feature fusion set ($p<0.05$). Also, SVR significantly increased the PCC^2 values compared to FFNN, when using the sEMG feature set ($p<0.05$), US imaging feature set ($p<0.05$), and sEMG-US imaging feature fusion set ($p<0.05$). Therefore, the results indicate the FFNN model may be more vulnerable to an over-fitting issue than the SVR model.

4 Discussion

This study investigated the benefits of using non-invasive neuromuscular signals fusion to predict volitional net plantarflexion moment based on the SVR and FFNN models. Our basic objective was to determine, on a personalized basis, the most appropriate sEMG time-domain feature and US imaging feature for predicting net plantarflexion moment. Our secondary

objective was to investigate whether the fusion of sEMG and US imaging features can improve the prediction accuracy. We determined the personalized dominant sEMG time-domain features and US imaging features from GAS and SOL muscles by using correlation analysis. We compared the net plantarflexion moment prediction performance with the sEMG-US imaging feature fusion set to sole sEMG feature set and sole US imaging feature set. The experimental results from nine able-bodied participants demonstrated the superior prediction performance by using the feature fusion set than using a sole sEMG feature set – an outcome that supported our hypothesis. However, we did not observe statistically significant improvement by using the feature fusion set over a sole US imaging feature set.

The neuromuscular signal features from sEMG and US imaging have been shown to correlate with measured joint kinetics and kinematics during isometric and non-isometric joint motion by using machine learning algorithms [27]–[29] or Hill-type neuromuscular model (HNM) approaches [11], [13], [30]. For machine learning algorithms, apart from SVR applied in this study, linear regression [11], [20], [31], artificial neural network [32]–[35], and Gaussian process regression [27], [36] are also well investigated. Compared to physics-based personalized neuromusculoskeletal models, such as in [11], [13], [30], machine learning is undoubtedly a powerful tool for identifying relationships between joint function and underlying neuromuscular signals, especially for the circumstance that multiple muscles co-contraction exists in the same muscle group. Moreover, machine learning approaches assume no underlying mechanistic representation of the physiological system, and it is always considered as a 'black box' of arbitrary, but sophisticated, organization [37], which simplifies the model calibration procedure given less requirement of physiological measures like mentioned in Hill-type neuromusculoskeletal model.

The five time-domain features extracted from the sEMG signal in this study are commonly used in the literature to understand and/or estimate joint moment/muscle force and joint movement [14], [38]. One critical parameter when extracting sEMG time-domain features is the window length. A longer window length could reduce the time domain feature’s noise and make the feature’s time sequence smoother, but it could also cause signal lag and fidelity loss. The choice of window length is a balance between sEMG feature smoothness and fidelity. Suitable window lengths from previously published studies ranged from 150 ms [39] to 500 ms [40]. The

mean correlation coefficients between each dominant sEMG time-domain feature and ankle net plantarflexion moment in this work ranged from 0.83 to 0.97. This range is within that previously reported in [41] (i.e., 0.77 to 0.99). In the current study, we applied the sEMG time-domain analysis [11], [13], [16], to simplify the signal processing procedures and make an emphasis on the benefit of fusing sEMG and US feature sets when predicting net plantarflexion moment. In future work, for sEMG signal processing, more nonlinear correlations will be considered and investigated, like cross-fuzzy entropy in [42]–[44]. The mean absolute correlation coefficients between each dominant US imaging feature and net plantarflexion moment ranged from 0.88 to 0.98, which is consistent with findings in prior publications [25], [29], [45], [46]. Compared to the aforementioned correlation coefficients between sEMG and net plantarflexion moment, the US imaging indicates a stronger linear correlation with the net plantarflexion moment. However, the results in Table 1 indicate that the dominant US imaging features are personalized among different participants, and it is hard to determine one or two general dominant US imaging feature(s) by using the correlation analysis.

Ankle posture-dependent variations in net plantarflexion MVIC moment reported here are consistent with muscle length-tension behavior [47]–[50]. Indeed, the selected ankle joint postures would elicit fascicle shortening from dorsiflexion to plantarflexion for both the biarticular GAS and uniarticular SOL, which likely explains the progressively smaller net plantarflexion MVIC moments shown in Fig. 4 across all participants. Also, the net plantarflexion MVIC moment varied from person to person, and this resulted in the higher variations of the SVR model-based prediction RMSE values in Fig. 7 across ankle joint postures and participants. So, the RMSE values normalized to the net plantarflexion moment at corresponding MVIC (NRMSE) would be beneficial for compromising those variations. Prediction results were considered excellent if the NRMSE value was smaller than 15% [33]. As shown in Fig. 8 and Fig. 9, in SVR (FFNN) model-based prediction, the mean NRMSE values using those three feature sets were all less than 13.5% (14.6%), especially the mean NRMSE value using the sEMG-US imaging feature fusion set is less than 8.5% (10.1%). These results indicate successful net plantarflexion moment prediction performance with the proposed sEMG-US imaging feature fusion set based on SVR and FFNN machine learning models.

During volitional joint movement, both an sEMG signal and a US imaging signal can be used to reflect the movement intent at the neuromuscular level and they provide complementary information [13]. Specifically, sEMG signals measure electric potentials generated by muscle motor units when neurally activated. The amplitude and density of sEMG signals linearly correlate with the number of firing neurons, which offers an indirect electrical measurement of action potential during the skeletal muscle contraction from a micro perspective [51]. Conversely, US imaging signals directly visualize skeletal muscle contractions from a morphological perspective [52]. Thus, the fusion between them can 1) mitigate unexpected cross-talk from neighboring muscles; and 2) lower the structural or functional feature drift caused by accumulated pixel displacements using the optimal flow tracking algorithms.

As a preliminary study with fused sEMG and US imaging dominant features for isometric plantarflexion, our results are promising. They can help overcome the challenges in volitional control of assistive devices, including FES and powered ankle exoskeleton. Since only able-bodied participants were included in the current study, future experiments on patients with plantar flexor impairment are needed to verify the implementations of the proposed neuromuscular model-free ankle joint moment prediction approach. In addition, the features extraction from sEMG signal and US imaging, SVR or FFNN model calibration, and prediction were performed offline in this study, however, due to the intensive computation for US imaging feature extraction, online implementation needs more advanced techniques, such as deep neural networks in [53], which needs more investigation in future work. One limitation in the current study is that the sEMG signal and US imaging signal of the GAS muscle did not come from the same head, although evidence suggests that sEMG signals from MG and LG are comparable [54]. Therefore, when performing the dominant neuromuscular feature fusion on the GAS muscle, we fused the US imaging dominant feature from MG and sEMG time-domain dominant feature from LG. Thus, we cannot exclude the possibility of higher than anticipated net plantarflexion moment calibration and prediction errors.

5 Conclusion

In this paper, we investigated the feasibility of using SVR and FFNN machine learning models and fused neuromuscular signals from sEMG and US imaging to predict ankle net plantarflexion moment during isometric contractions. The SVR model-based prediction results showed that using the sEMG-US feature fusion set and sole US feature set, the NRMSE values were significantly smaller, and the PCC^2 values were significantly larger than that using the sole sEMG feature set. However, we did not observe statistically significant improvement using the feature fusion set over the sole US imaging feature set. The FFNN model-based prediction results showed that using the sEMG-US feature fusion set, the NRMSE values were significantly smaller, and the PCC^2 values were significantly larger than that using the sole sEMG feature set and sole US feature set. However, we did not observe a statistically significant difference using the sole sEMG feature set and sole US imaging feature set. The improved ankle net plantarflexion moment prediction precision can be potentially applied to dynamic locomotor tasks such as walking. Ultimately, this work could lead to improvements in volitional control of assistive devices, including human ankle joint motion intent detection, improved intuitiveness, and assist-as-needed control.

Acknowledgments

We thank Natalie Fragnito for her proofreading of the article. This work was supported by National Science Foundation Career award # 1750748.

References

[1] T. W. P. Huang, K. A. Shorter, P. G. Adamczyk, and A. D. Kuo, “Mechanical and energetic consequences of reduced ankle plantar-flexion in human walking,” *J. Exp. Biol.*, vol. 218, no. 22, pp. 3541–3550, Nov. 2015.

[2] D. P. Ferris and C. L. Lewis, “Robotic lower limb exoskeletons using proportional myoelectric control,” in *Proceedings of the 31st Annual International Conference of the IEEE Engineering in Medicine and Biology Society: Engineering the Future of Biomedicine, EMBC 2009*, 2009, vol. 2009, pp. 2119–2124.

[3] R. Jiménez-Fabián and O. Verlinden, “Review of control algorithms for robotic ankle systems in lower-limb orthoses, prostheses, and exoskeletons,” *Med. Eng. Phys.*, vol. 34,

no. 4, pp. 397–408, May 2012.
[4] K. Z. Takahashi, M. D. Lewek, and G. S. Sawicki, “A neuromechanics-based powered ankle exoskeleton to assist walking post-stroke: A feasibility study,” *J. Neuroeng. Rehabil.*, vol. 12, no. 1, pp. 1–13, Feb. 2015.
[5] D. G. Embrey, S. L. Holtz, G. Alon, B. A. Brandsma, and S. W. McCoy, “Functional Electrical Stimulation to Dorsiflexors and Plantar Flexors During Gait to Improve Walking in Adults With Chronic Hemiplegia,” *Arch. Phys. Med. Rehabil.*, vol. 91, no. 5, pp. 687–696, May 2010.
[6] T. M. Kesar *et al.*, “Functional electrical stimulation of ankle plantarflexor and dorsiflexor muscles: effects on poststroke gait.,” *Stroke*, vol. 40, no. 12, pp. 3821–7, Dec. 2009.
[7] S. Srivastava *et al.*, “Assist-as-Needed Robot-Aided Gait Training Improves Walking Function in Individuals Following Stroke,” *IEEE Trans. Neural Syst. Rehabil. Eng.*, vol. 23, no. 6, pp. 956–963, Nov. 2015.
[8] S. Hussain, P. K. Jamwal, M. H. Ghayesh, and S. Q. Xie, “Assist-as-needed control of an intrinsically compliant robotic gait training orthosis,” *IEEE Trans. Ind. Electron.*, vol. 64, no. 2, pp. 1675–1685, 2017.
[9] Q. Zhang, L. Teng, Y. Wang, T. Xie, and X. Xiao, “A Study of Flexible Energy-Saving Joint for Biped Robots Considering Sagittal Plane Motion,” in *Lecture Notes in Computer Science (including subseries Lecture Notes in Artificial Intelligence and Lecture Notes in Bioinformatics)*, 2015, vol. 9245, pp. 333–344.
[10] D. Zanotto, Y. Akiyama, P. Stegall, and S. K. Agrawal, “Knee Joint Misalignment in Exoskeletons for the Lower Extremities: Effects on User’s Gait,” *IEEE Trans. Robot.*, vol. 31, no. 4, pp. 978–987, Aug. 2015.
[11] Q. Zhang, A. Iyer, K. Kim, and N. Sharma, “Evaluation of Non-Invasive Ankle Joint Effort Prediction Methods for Use in Neurorehabilitation Using Electromyography and Ultrasound Imaging,” *IEEE Trans. Biomed. Eng.*, pp. 1–1, Aug. 2020.
[12] M. Sartori, D. Farina, and D. G. Lloyd, “Hybrid neuromusculoskeletal modeling to best track joint moments using a balance between muscle excitations derived from electromyograms and optimization,” *J. Biomech.*, vol. 47, no. 15, pp. 3613–3621, Nov. 2014.
[13] Q. Zhang, K. Kim, and N. Sharma, “Prediction of Ankle Dorsiflexion Moment by Combined Ultrasound Sonography and Electromyography,” *IEEE Trans. Neural Syst. Rehabil. Eng.*, vol. 28, no. 1, pp. 318–327, 2020.
[14] J. Han, Q. Ding, A. Xiong, and X. Zhao, “A state-space EMG model for the estimation of continuous joint movements,” *IEEE Trans. Ind. Electron.*, vol. 62, no. 7, pp. 4267–4275, Jul. 2015.
[15] D. L. Crouch, L. Pan, W. Filer, J. W. Stallings, and H. Huang, “Comparing surface and intramuscular electromyography for simultaneous and proportional control based on a musculoskeletal model: A pilot study,” *IEEE Trans. Neural Syst. Rehabil. Eng.*, vol. 26, no. 9, pp. 1735–1744, Sep. 2018.
[16] L. J. Hargrove, K. Englehart, and B. Hudgins, “A comparison of surface and intramuscular myoelectric signal classification,” *IEEE Trans. Biomed. Eng.*, vol. 54, no. 5, pp. 847–853, May 2007.
[17] E. M. Strasser, T. Draskovits, M. Praschak, M. Quittan, and A. Graf, “Association between

ultrasound measurements of muscle thickness, pennation angle, echogenicity and skeletal muscle strength in the elderly," *Age (Omaha).*, vol. 35, no. 6, pp. 2377–2388, 2013.

[18] A. Arampatzis, K. Karamanidis, S. Stafilidis, G. Morey-Klapsing, G. DeMonte, and G. P. Brüggemann, "Effect of different ankle- and knee-joint positions on gastrocnemius medialis fascicle length and EMG activity during isometric plantar flexion," *J. Biomech.*, vol. 39, no. 10, pp. 1891–1902, 2006.

[19] D. L. Damiano, L. A. Prosser, L. A. Curatalo, and K. E. Alter, "Muscle plasticity and ankle control after repetitive use of a functional electrical stimulation device for foot drop in cerebral palsy.," *Neurorehabil. Neural Repair*, vol. 27, no. 3, pp. 200–7.

[20] J.-Y. Guo, Y.-P. Zheng, H.-B. Xie, and X. Chen, "Continuous monitoring of electromyography (EMG), mechanomyography (MMG), sonomyography (SMG) and torque output during ramp and step isometric contractions," *Med. Eng. Phys.*, vol. 32, no. 9, pp. 1032–1042, Nov. 2010.

[21] A. S. Dhawan *et al.*, "Proprioceptive Sonomyographic Control: A novel method for intuitive and proportional control of multiple degrees-of-freedom for individuals with upper extremity limb loss," *Sci. Rep.*, vol. 9, no. 1, Dec. 2019.

[22] Z. Sheng, N. Sharma, and K. Kim, "Quantitative Assessment of Changes in Muscle Contractility Due to Fatigue during NMES: An Ultrasound Imaging Approach," *IEEE Trans. Biomed. Eng.*, vol. 67, no. 3, pp. 832–841, Mar. 2020.

[23] S. Sikdar *et al.*, "Novel method for predicting dexterous individual finger movements by imaging muscle activity using a wearable ultrasonic system," *IEEE Trans. Neural Syst. Rehabil. Eng.*, vol. 22, no. 1, pp. 69–76, Jan. 2014.

[24] H. Drucker *et al.*, "Support vector regression machines Queueing View project banded symmetric indefinte matrices View project Support Vector Regression Machines," 1997.

[25] X. Chen, Y. P. Zheng, J. Y. Guo, Z. Zhu, S. C. Chan, and Z. Zhang, "Sonomyographic responses during voluntary isometric ramp contraction of the human rectus femoris muscle," *Eur. J. Appl. Physiol.*, vol. 112, no. 7, pp. 2603–2614, Jul. 2012.

[26] D. J. Farris and G. A. Lichtwark, "UltraTrack: Software for semi-automated tracking of muscle fascicles in sequences of B-mode ultrasound images," *Comput. Methods Programs Biomed.*, vol. 128, pp. 111–118, May 2016.

[27] M. H. Jahanandish, N. P. Fey, and K. Hoyt, "Lower-Limb Motion Estimation Using Ultrasound Imaging: A Framework For Assistive Device Control," *IEEE J. Biomed. Heal. Informatics*, pp. 1–1, Jan. 2019.

[28] A. Phinyomark, P. Phukpattaranont, and C. Limsakul, "Feature reduction and selection for EMG signal classification," *Expert Syst. Appl.*, vol. 39, no. 8, pp. 7420–7431, Jun. 2012.

[29] Jun Shi *et al.*, "Continuous Monitoring of Sonomyography, Electromyography and Torque Generated by Normal Upper Arm Muscles During Isometric Contraction: Sonomyography Assessment for Arm Muscles," *IEEE Trans. Biomed. Eng.*, vol. 55, no. 3, pp. 1191–1198, Mar. 2008.

[30] T. J. M. Dick, A. A. Biewener, and J. M. Wakeling, "Comparison of human gastrocnemius forces predicted by Hill-type muscle models and estimated from ultrasound images," *J. Exp. Biol.*, vol. 220, no. 9, pp. 1643–1653, May 2017.

[31] T. Suzuki, R. Kinugasa, and S. Fukashiro, "Activation of plantar flexor muscles is

constrained by multiple muscle synergies rather than joint torques," *PLoS One*, vol. 12, no. 11, p. e0187587, Nov. 2017.

[32] R. J. Cunningham, P. J. Harding, I. D. Loram, F. A. Author, S. B. Author, and T. C. Author, "The application of deep convolutional neural networks to ultrasound for modeling of dynamic states within human skeletal muscle," *bioRxiv*. 28-Jun-2017.

[33] M. M. Liu, W. Herzog, and H. H. C. M. Savelberg, "Dynamic muscle force predictions from EMG: an artificial neural network approach," *J. Electromyogr. Kinesiol.*, vol. 9, no. 6, pp. 391–400, Dec. 1999.

[34] F. Sepulveda, D. M. Wells, and C. L. Vaughan, "A neural network representation of electromyography and joint dynamics in human gait," *J. Biomech.*, vol. 26, no. 2, pp. 101–109, Feb. 1993.

[35] W. Youn and J. Kim, "Estimation of elbow flexion force during isometric muscle contraction from mechanomyography and electromyography," *Med. Biol. Eng. Comput.*, vol. 48, no. 11, pp. 1149–1157, Nov. 2010.

[36] Q. Zhang, A. Iyer, K. Kim, and N. Sharma, "Volitional Contractility Assessment of Plantar Flexors by Using Non-invasive Neuromuscular Measurements," in *Proceedings of the IEEE RAS and EMBS International Conference on Biomedical Robotics and Biomechatronics*, 2020, vol. 2020-November, pp. 515–520.

[37] D. J. Saxby *et al.*, "Machine learning methods to support personalized neuromusculoskeletal modelling," *Biomech. Model. Mechanobiol.*, vol. 19, no. 4, pp. 1169–1185, Aug. 2020.

[38] A. Alkan and M. Günay, "Identification of EMG signals using discriminant analysis and SVM classifier," *Expert Syst. Appl.*, vol. 39, no. 1, pp. 44–47, Jan. 2012.

[39] O. W. Samuel *et al.*, "Pattern recognition of electromyography signals based on novel time domain features for amputees' limb motion classification," *Comput. Electr. Eng.*, vol. 67, pp. 646–655, Apr. 2018.

[40] A. Georgakis, L. K. Stergioulas, and G. Giakas, "Fatigue analysis of the surface EMG signal in isometric constant force contractions using the averaged instantaneous frequency," *IEEE Trans. Biomed. Eng.*, vol. 50, no. 2, pp. 262–265, Feb. 2003.

[41] O. Mohamed, J. Perry, and H. Hislop, "Relationship between wire EMG activity, muscle length, and torque of the hamstrings," *Clin. Biomech.*, vol. 17, no. 8, pp. 569–579, Oct. 2002.

[42] H. B. Xie, Y. P. Zheng, J. Y. Guo, and X. Chen, "Cross-fuzzy entropy: A new method to test pattern synchrony of bivariate time series," *Inf. Sci. (Ny).*, vol. 180, no. 9, pp. 1715–1724, May 2010.

[43] H. B. Xie, B. Sivakumar, T. W. Boonstra, and K. Mengersen, "Fuzzy entropy and its application for enhanced subspace filtering," *IEEE Trans. Fuzzy Syst.*, vol. 26, no. 4, pp. 1970–1982, Aug. 2018.

[44] H. Azami, P. Li, S. E. Arnold, J. Escudero, and A. Humeau-Heurtier, "Fuzzy entropy metrics for the analysis of biomedical signals: Assessment and comparison," *IEEE Access*, vol. 7, pp. 104833–104847, 2019.

[45] F. Ateş *et al.*, "Muscle shear elastic modulus is linearly related to muscle torque over the entire range of isometric contraction intensity," *J. Electromyogr. Kinesiol.*, vol. 25, no. 4, pp. 703–708, Aug. 2015.

[46] K. Bouillard, A. Nordez, P. W. Hodges, C. Cornu, and F. Hug, “Evidence of changes in load sharing during isometric elbow flexion with ramped torque,” *J. Biomech.*, vol. 45, no. 8, pp. 1424–1429, May 2012.
[47] B. C. Abbott and X. M. Aubert, “The force exerted by active striated muscle during and after change of length,” *J. Physiol.*, vol. 117, no. 1, p. 77, 1952.
[48] T. S. Buchanan, D. G. Lloyd, K. Manal, and T. F. Besier, “Neuromusculoskeletal Modeling: Estimation of Muscle Forces and Joint Moments and Movements from Measurements of Neural Command,” *J. Appl. Biomech.*, vol. 20, no. 4, pp. 367–395, Nov. 2004.
[49] J. Paquin and G. A. Power, “History dependence of the EMG-torque relationship,” *J. Electromyogr. Kinesiol.*, vol. 41, pp. 109–115, Aug. 2018.
[50] H. B. Xie, Y. P. Zheng, J. Y. Guo, X. Chen, and J. Shi, “Estimation of wrist angle from sonomyography using support vector machine and artificial neural network models,” *Med. Eng. Phys.*, vol. 31, no. 3, pp. 384–391, Apr. 2009.
[51] M. Barbero, R. Merletti, and A. Rainoldi, *Atlas of muscle innervation zones: understanding surface electromyography and its applications*. 2012.
[52] P. Aagaard *et al.*, “A mechanism for increased contractile strength of human pennate muscle in response to strength training: changes in muscle architecture,” *J. Physiol.*, vol. 534, no. 2, pp. 613–623, Jul. 2001.
[53] R. L. Krupenevich, C. J. Funk, and J. R. Franz, “Automated analysis of medial gastrocnemius muscle-tendon junction displacements during isolated contractions and walking using deep neural networks,” *bioRxiv*. bioRxiv, p. 2020.09.29.317529, 01-Oct-2020.
[54] L. Mademli, A. Arampatzis, G. Morey-Klapsing, and G. P. Brüggemann, “Effect of ankle joint position and electrode placement on the estimation of the antagonistic moment during maximal plantarflexion,” *J. Electromyogr. Kinesiol.*, vol. 14, no. 5, pp. 591–597, Oct. 2004.